Laboratory experiment on the impact of wind on water turbulence in shallow areas

Yao, Peng; Pu, Jinshan; Chen, Yongping; Su, Min; Stive, Marcel J.F.; Wang, Zhengbing

DOI
10.1016/j.coastaleng.2025.104765

Publication date
2025

Document Version
Final published version

Published in
Coastal Engineering

Citation (APA)
Yao, P., Pu, J., Chen, Y., Su, M., Stive, M. J. F., & Wang, Z. (2025). Laboratory experiment on the impact of wind on water turbulence in shallow areas. *Coastal Engineering*, *200*, Article 104765. https://doi.org/10.1016/j.coastaleng.2025.104765

Coastal Engineering 200 (2025) 104765

Contents lists available at ScienceDirect

Coastal Engineering

journal homepage: www.elsevier.com/locate/coastaleng

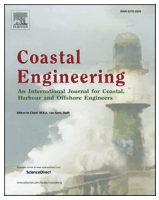

Laboratory experiment on the impact of wind on water turbulence in shallow areas

Peng Yao [a,b,1], Jinshan Pu [c,1], Yongping Chen [a,c,*], Min Su [c], Marcel J.F. Stive [d], Zhengbing Wang [d,e]

[a] National Key Laboratory of Water Disaster Prevention, Hohai University, Nanjing, 210098, China
[b] Key Laboratory of Ocean Space Resource Management Technology, MNR, China
[c] College of Harbour, Coastal and Offshore Engineering, Hohai University, 1 Xikang Road, Nanjing, 210098, China
[d] Faculty of Civil Engineering and Geosciences, Section of Hydraulic Engineering, Delft University of Technology, P.O. Box 5048, 2600, GA, Delft, the Netherlands
[e] Deltares, P.O. Box 177, 2600, MH, Delft, the Netherlands

ARTICLE INFO

Keywords:
Water turbulence
Wind effects
TKE
Shallow water
Laboratory experiment

ABSTRACT

A series of laboratory experiments focused on the wind impact on the vertical turbulence structure in shallow water has been carried out. The turbulence characteristics in the mid-lower water column under relatively strong wave conditions are investigated. For different experimental conditions (i.e., waves only, wind only, combinations of wind and waves) in a wind-wave flume, the effects of wind and waves were investigated in detail by decomposing the total energy into different terms (i.e., wind-driven currents, wind waves, wind-induced turbulence). The results show that shallow water waves play a major role in transferring energy by non-zero wave-induced Reynolds stress ($\overline{\tilde{u}\tilde{w}}$), turbulent diffusion ($\overline{u'w'}$). The superimposed wind can further modify the energy transference due to its impact on wave asymmetry and skewness as well as through homogenizing the time-average velocity profiles. Subsequently, the impact of wind on turbulence structure was explored in detail. The most important finding is that the wind can directly influence water turbulent diffusion ($\overline{u'w'}$) along with wave-induced turbulence. The vertical turbulence intensity (σ_w) is more sensitive to wind than the horizontal turbulence intensity (σ_u). Furthermore, the major way that wind affects water turbulence is by introducing nonlinear wind and wave interactions, which exhibit a maximum effect (~60 % compared to the respective effect of wind and wave) at the edge of the bottom boundary layer. This study demonstrates that the wind can transfer momentum downward to mid-lower water columns even under strong waves in shallow waters, which differs from that in deep water systems.

1. Introduction

In the marine environment, water turbulence is simultaneously influenced by waves, winds and currents, affecting water mixing processes and influencing transport processes of gas, heat, nutrients and sediment (Thais and Magnaudet, 1996; Rainville and Woodgate, 2009; Rainville et al., 2011; Nishino et al., 2020). Such processes are of great practical significance in exploring marine environmental changes as well as coastal morphological evolution. In natural water systems, wave, wind and current are often coexisting, performing together or on each other to influence the water turbulence and mixing processes (Hatori et al., 1981; Imai et al., 1981; Nielsen and Teakle, 2004; Qiao et al., 2016). That is, wave, wind and current can all contribute to water turbulence.

Various studies have demonstrated that water waves contribute to turbulence in the water column using field measurements (Cavaleri and Zecchetto, 1987; Gemmrich and Farmer, 2004; Babanin, 2006; Garett and Gemmrich, 2009) and laboratory experiments (Kemp and Simons, 1982, 1983; Bliven et al., 1984; Jiang et al., 1990; Thais and Magnaudet, 1995; Dai et al., 2010; Savelyev et al., 2012; Smeltzer et al., 2023). In laboratory experiments, Kemp and Simons (1982) reported that the turbulence intensities averaged over the wave cycle are increased by the superposition of waves on a current in the same direction. Later on, they detected the same phenomenon in another experiment, in which the

* Corresponding author. National Key Laboratory of Water Disaster Prevention, Hohai University, Nanjing, 210098, China.
E-mail address: ypchen@hhu.edu.cn (Y. Chen).
[1] These authors have contributed equally to this work.

https://doi.org/10.1016/j.coastaleng.2025.104765
Received 6 February 2025; Received in revised form 2 April 2025; Accepted 23 April 2025
Available online 27 April 2025

wave propagating against the current, and turbulence intensities and Reynolds stresses vary through the wave cycle near the rough bed, with peak values far over those experienced by currents alone, but of the same order as for waves alone (Kemp and Simons, 1983). Bliven et al. (1984) found that the Reynolds stress and the turbulent energy of the water column increased with the wave steepness and decayed exponentially with water depth. Savelyev et al. (2012) discovered that the turbulence kinetic energy (*TKE*) is a function of wave steepness, wave phase and initial turbulent conditions and verified it by numerical methods. For the field measurements, Cavaleri and Zecchetto (1987) conducted thorough measurements for the wave-induced Reynolds stresses on the coast of Venice, concluding that the non-zero vertical momentum fluxes are evident under non-breaking wave and the magnitude of the fluxes appear to depend quadratically on the height of individual waves.

Some numerical studies also provided evidence of wave-induced turbulence (Fulgosi et al., 2003; Qiao et al., 2004, 2008, 2016; Guo and Shen, 2013; Xuan and Shen, 2023; Fujiwara, 2024). For example, Teixeira and Belcher (2002) developed a rapid-distortion model to explore the interaction of weak turbulence with a monochromatic irrotational surface water wave, concluding the variation of streamwise and normal Reynolds stress within a wave period and verified the experimental results of Thais and Magnaudet (1996). Qiao et al. (2004, 2008) made improvements in predictions of the upper ocean thermal structure and mixed layer depth compared to the traditional mixing schemes by introducing nonbreaking wave-induced stress in ocean circulation models coupled with surface waves. Guo and Shen (2013) discovered that the interaction of wave-turbulence depends on wave nonlinearity and the time scale ratio between them by direct numerical simulation, and then quantified the Lagrange properties and explored the cumulative wave effect on turbulence.

In addition to the wave-induced turbulence, extensive studies also concentrated on the wind effect on turbulence. Lin and Gad-el-Hak (1984) reported that both wind and waves can contribute to the turbulence in the water column by laboratory conditions. They suggested that wind can still contribute to water turbulence at certain depths, where the effects of orbital wave motion disappear. Cheung and Street (1988) suggested a coupling relationship between wave and turbulence by wind-wave combined laboratory experiments. Wei et al. (2018) found that the turbulent Reynolds stress decreases with the increasing water depth and the wind waves (generated by wind blowing), compared to swell (generated mechanically by a paddle in a flume), are more effective in activating turbulence by investigating the Reynolds stress and the turbulence dissipation rate. Olfateh et al. (2017) studied the wave-induced Reynolds stress $\widetilde{\tilde{u}\tilde{w}}$ in two more detailed series of laboratory experiments, presenting physical mechanisms of the generation of non-zero $\widetilde{\tilde{u}\tilde{w}}$ which was previously neglected. Addona et al. (2020, 2023, 2024) conducted a series of experimental studies on interactions of wave and opposing wind. They found that wave reflection suppresses the downward propagation of water turbulence, involving complex nonlinear interactions.

As described above, it is known that wind can directly affect water turbulence in addition to waves. The wind impacts on turbulence decrease with the increasing distance from the water surface and eventually diminish at a certain elevation. Part of the existing research on the effects of wind on turbulence is focused on the air-water interfaces in deep waters (e.g., oceans), where the $h/L \geq 0.5$ (h represents water depth and L represents wavelength) (Bosboom and Stive, 2021). In such areas, the relative wave height (H/h, and H is wave height) is usually very small (Table 1). In the areas with intermediate and shallow water depth ($h/L < 0.5$), wind could affect wave shape and influence water turbulence significantly (Zdyrski and Feddersen, 2022). Related studies have focused on coastal moderate waves, i.e., the relative wave heights (H/h) are less than 0.1 and the bed shear stresses are below 0.16 Pa (Olfateh et al., 2017; Addona et al., 2018; see Table 1). Meanwhile, most existing studies have focused on the turbulence characteristics within the mid-upper water column.

Table 1
Summary of the experimental conditions of previous research. H represents the wave height, h represents the water depth, L represents the wavelength, U_∞ represents the reference wind speed and τ_b is the bed shear stress.

Research	H/h	U_∞(m s^{-1})	h/L	τ_b(pa)
Hatori et al. (1981)	0.0092–0.058	7.5,10	0.79–1.28	≈0
Cheung and Street (1988)	0.044	1.7–6.2	0.67	≈0
Thais and Magnaudet (1996)	0.054	3.0–5.8	0.59	≈0
Wei et al. (2018)	0.018–0.034	12–21	1.10–2.05	≈0
Olfateh et al. (2017)	0.03–0.09	9–16.5	0.29–1.03	0.03–0.14
Addona et al. (2018)	0.074–0.10	3.65–7.65	0.21	0.09–0.16
Present research	0.133–0.4	0–6	0.13	0.26–0.52

In coastal shallow waters, turbulence characteristics in the mid-lower water column are critical for sediment resuspension (Feddersen and Veron, 2005; Sous et al., 2020). Therefore, it is important to gain knowledge regarding the effects of wind-wave interactions on near-bottom turbulence. Existing research is primarily focused on turbulence near-bottom wave boundary layer (e.g., Nielsen, 1992; Fredsøe et al., 2003; Henriquez et al., 2014) and wave-breaking related turbulence near the water surface (e.g., Agrawal et al., 1992; Feddersen et al., 2007; Feddersen, 2012; Moghimi et al., 2016), which is common in sandy beach. If considering wind, an onshore wind could make wave breaking ahead of time and enhance the *TKE* near the water surface (Liu et al., 2016; Jiang et al., 2020; Zdyrski and Feddersen, 2022). Due to the flat bottom and wide width, wave propagation over tidal flats is different from sandy beaches. Especially, the increase of water depth on tidal flats during rough weather, allows a relatively wide area with non-breaking waves (Zhang et al., 2021) leading to strong dynamic conditions, which is important for sediment resuspension. To this end, this research primarily concentrates on high-intensity waves (e.g., H/h of 0.133–0.4 and bed shear stress of 0.26–0.52; see Table 1) and the combined effects of wind-wave interactions on turbulence in the mid-lower water layers.

The main objective of this study is to investigate the wind effect on the turbulence structure under high-intensity non-breaking waves in shallow waters (i.e., tidal flats). To this end, a series of laboratory experiments have been designed and carried out using mechanically generated waves (larger relative wave heights) and surface blowing winds. The addressed scientific questions are (1) to what extent and (2) how wind influences the high-intensity wave-induced turbulence in shallow areas. Since water turbulence plays a substantial role in fine-grained sediment suspension and transport, especially in rough weather conditions, understanding the contribution of wind to the turbulence can shed light on suspended sediment dynamics in shallow areas.

2. Theoretical background

Wind can generate water waves by blowing over a water surface, which consequently influences water turbulence, and transfers energy downward energy from the atmosphere into water. That is, the wind energy can be injected into water exerting influences on water movement in different ways and different spatial-temporal scales, e.g., wind-driven currents, wind waves, turbulence. Viscous and Reynolds stresses, which are major representations that transfer momentum vertically from the atmosphere to the sea, contribute to the total shear stresses in the following formulations in an x-z plane (Reynolds and Hussain, 1972; Benilov et al., 1974; Cheung and Street, 1988; Mellor, 2013; Olfateh et al., 2017):

$$\tau_{xz} = \mu \frac{du}{dz} - \rho\widetilde{\tilde{u}\tilde{w}} - \rho\overline{u'w'} \tag{1}$$

$$u = \overline{u} + \widetilde{u} + u' \tag{2}$$

$$w = \overline{w} + \widetilde{w} + w' \tag{3}$$

where, μ is the fluid dynamic viscosity; ρ is the fluid density, respectively; u and w are the instantaneous velocity in the horizontal and vertical direction, respectively ; $\overline{u}$ and $\overline{w}$ are the time-averaged component of u and w, respectively; $\widetilde{u}$ and $\widetilde{w}$ are the periodical components; u' and w' represent the turbulent fluctuations.

The first term of the left hand in Eq. 1 ($\mu \frac{du}{dz}$) represents the viscous effect, the second term (i.e., $-\rho\overline{\widetilde{u}\widetilde{w}}$) represents the wave Reynolds stress and the last one ($-\rho\overline{u'w'}$) denotes the turbulent Reynolds stress. In addition to these three terms, Olfateh et al. (2017) suggested that the wind-driven circulations, represented by $\overline{uw}$, play also a significant role in momentum transfer at elevations not adjacent to the surface and bed boundaries.

The water turbulence (e.g., $\overline{u'w'}$) is not only a component of momentum transfer by winds, but also plays a significant role in mixing processes in the water column. By summarizing existing studies, water turbulence can be influenced by wind (Thais and Magnaudet, 1996), waves (Feddersen, 2012), and bottom boundary layer dynamics (Henriquez et al., 2014). In deep waters, turbulence mainly affects the mixing of surface waters, and this effect gradually diminishes downward (Qiao et al., 2004). However, in shallow waters, turbulence affects the mixing process throughout the entire water depth, where surface turbulence is mainly enhanced by wave-breaking processes (Feddersen and Trowbridge, 2005), while bottom turbulence is influenced by the bottom boundary layer dynamics (Nielsen, 1992).

Given the complexity of the impact of wind on water turbulence in shallow areas, there are still many unresolved issues. For example, the interactions of these aforementioned factors of influence (wind, waves, bottom boundary layer, etc.) on water turbulence, are unclear. In this study, we aim to explore characteristics of water turbulence under nonbreaking waves over flat bottom, and how the external wind influences the wave-induced turbulence. For this purpose, we have designed a series of wind-wave flume experiments, including wind-only, wave-only and wind-wave combined conditions, to separate the effects on turbulence of different factors.

3. Experimental set up and data analysis

3.1. Flume experimental setup

The laboratory experiments were performed in the wind-wave flume in Hohai University, China. The flume is 80m long, 1m wide and 1.5m high (Fig. 1a), which was equipped with a wave generator to generate gravity waves. A suction fan was installed at the opposite side of the wave generator to generate the onshore wind which is in the same direction as gravity wave (Yao et al., 2015; Chen et al., 2023). That is, the wave generator was located at the upstream end of the flume, while the wind maker was set at the downstream end. The wave generator functioned with an active absorption feature. The secondary waves can be detected by wave height probes installed on the wave paddle and minimized by automatic paddle position adjusting. The gravel beach slope (1:4.5) was installed at the downstream end to dissipate the wave reflection. According to Addona et al. (2018), wave reflection can suppress the momentum transfer of wind to wave. In our experiments, the reflection coefficients were calculated to be 0.06–0.08 under wave conditions with wave heights of 6 cm–12 cm and a period of 1.5 s based on the 3-gauge method of Mansard and Funke (1980). The minimal variation of reflection coefficients of different wave conditions suggests a consistency of reflection influence on wind-induced turbulence. The wind covers are fixed on the top of the flume. The wind velocity, up to 6 ms^{-1}, was controlled by means of altering the variable frequency of the suction fan.

The water surface elevation was measured by 4 wave gauges along the flume (Fig. 1a). The mean wave height was computed by averaging the data of the 4 wave gauges. The wind velocity was recorded by a hot-wire anemometer, which was located 35 cm above the still water surface. This elevation for wind velocity measurement was outside of the wind boundary layer according to previous studies that have similar experimental settings (Lai and Shemdin, 1971; Longo, 2012; Su et al., 2015). Thus, the recorded wind velocity can be regarded as being in the free stream zone.

Given the structural constraints of the wind tunnel, we employed ADV as the flow velocity measurement device due to its flexible deployment capabilities. The water velocity was measured by the Acoustic Doppler Velocimeter (ADV) which was placed on the top beam of the flume. Two same ADVs were placed in the flume to ensure data repeatability. In general, two ADV produced similar results, so only the results of the left ADV were used in this study. Vertical positioning of the ADV can be manipulated by a computer control system to measure the velocity profile. The sampling area is 5 cm below the ADV probe, avoiding interfering velocity profile there (Fig. 1b). It is difficult to investigate the turbulence in a strict sense because of the sampling frequency setting and ADV measurement volume, therefore, the turbulence analyzed in the present paper refers to the macroturbulence and its related structure. In total, 7 measurement points were arranged along the beam, the lowest one was 0.6 cm above the bottom, while the highest one was at Z=0.6h (h is the water depth), and the other 5 points were placed at every 0.1h in between. The sampling rate was set to 50Hz. It should be noted that the velocity signal near the water surface, which is a blind area of the ADV, cannot be recorded. Since several existing studies have suggested that wave Reynolds stress decreases from the water surface downward with a hyperbolic shape (e.g., Olfateh et al., 2017), we focused more on wind effects on the middle and bottom layers. Therefore, in this study, the turbulence structure in the middle and lower layers is analyzed and investigated.

3.2. Experimental conditions

In the experiment, different combinations of waves (wave heights, H = 6–12 cm) and winds (wind speed, U_0 = 0–6 m s^{-1}) were used. The

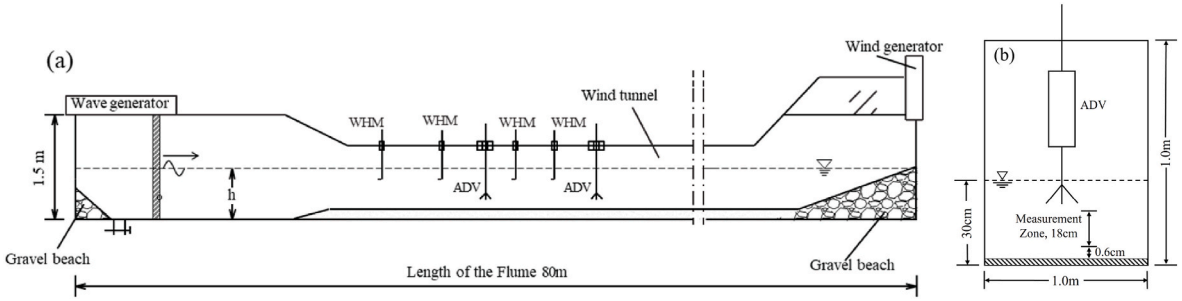

Fig. 1. (a) Layout of the wind-wave flume; (b) the cross section of ADV area.

wind effect on the water column can be obtained by a comparison between paddle wave-only (i.e., zero wind speed) and the combined cases (non-zero wind speed). A wind-only case (no paddle waves) was also conducted for comparison. The water depth h is kept to be 30 cm. The period of the paddle wave was chosen constant ($T = 1.5$s) throughout the whole set of experimental runs. The experimental results suggested that the wind-wave achieved equilibrium in 15–20 min and thus the data recording by instruments was started at 30 min after the beginning of the wave maker. In all experimental conditions, the waves were no breaking. The shallowness parameter (kh) of the experimental condition is about 0.8.

3.3. Scaling strategy

According to the mentioned experimental settings, our main motivation is exploring the wind influence mechanism on water turbulence in shallow areas rather than restoring the natural coastal environment accurately, but we still provide the scaling here as a reference on the wind and wave conditions in the field. The Reynolds number of the A0 is estimated to be 7 600 using:

$$Re = \frac{uL}{\nu} \tag{4}$$

Where the u is the water velocity, the L is the hydraulic radius of the experimental flume, and ν represents the kinematic viscosity coefficient, overtaking the critical number for laminar flow and turbulence flow (around 4 000). Therefore, we applied the Froude similitude in this study.

Subsequently, taking the tidal flat of the central Jiangsu coast as a reference site, the mean water depth (defined as h_f) was 7–10 m during rough weather (e.g., storm surge period). The water depth (h_l) in the laboratory flume was set constant as 0.3 m and thus the length scale (λ_l) was 23–33. Following Froude number scaling, the velocity scale ($\lambda_u = \sqrt{\lambda_l}$) and time scale ($\lambda_t = \sqrt{\lambda_l}$) were 4.8–5.8. Hence, given the experimental conditions listed in Table 2, the wave height was 0.06–0.12m, the wave period was 1.5 s and the wave speed was 1.5–6 m s^{-1}, representing wave heights of 1.4–4.0 m, wave periods of 7.2–8.7 s and wind speeds of 7.2–34.8 m s^{-1} in the field.

3.4. Data analyses

Data processing, on the one hand, includes statistical analyses of physical quantities, such as mean wave height of the different wave conditions, vertical distribution of mean flow velocity, and near-bed orbital velocity. Thus, hydrodynamic features of different wind-wave coupling conditions can be obtained and analyzed. On the other hand, turbulence parameters representing water turbulence under different conditions were also analyzed. Firstly, the turbulence component was separated from the original velocity signal. Subsequently, the turbulence parameters, such as Reynolds stress, turbulence intensity and TKE, were estimated. Detailed processes on turbulence extraction were listed as follows.

To investigate the variation of the water turbulence characteristics, the time-averaged and periodical components of u and w must be eliminated. Various methods have been developed to decompose raw velocity data and to obtain turbulence velocities, such as the tenth-order Butterworth filter method (Hooshmand et al., 2015; Lamb, 2004), the numerical bandpass filter (Meirelles et al., 2015; Savelyev et al., 2011), the linear filtering technique and triple decomposition method (Olfateh et al., 2017), the inertial subrange of the Kolmogorov spectrum (Soulsby and Humphery, 1990; Talke and Stacey, 2003; Longo, 2012; Wei et al., 2018), the DMD method (Chávez-Dorado et al., 2024), the EMD method (Peruzzi et al., 2021), nonlinear water wave decomposition technique (Jiang et al., 1990) and the phase-average method (Thais and Magnaudet, 1996; Su et al., 2015; Qiao et al., 2016; Addona et al., 2018).

In this study, due to different combinations of winds and waves, different approaches were chosen to obtain the turbulence parameters. For the wave-only and wind-wave combined cases, the phase-averaged method was used (Ardhuin and Jenkins, 2006; Su et al., 2015; Addona et al., 2018). For the wind-only case, the phase-averaged method is not applicable because the wind-induced waves were irregular for short periods. An energy spectrum analysis method which has been widely used in previous studies was adopted to separate the turbulence component from the velocity data of the wind-only case. The influence of different methods on the extraction of turbulence is discussed in the Discussion section.

Regarding the phase-average method, the turbulent velocity (e.g., in the horizontal direction) can be decomposed using (for the wave-only and wind-wave combined cases):

$$\langle u \rangle = \frac{1}{N}\sum_{n=0}^{N-1} u(t+nT), \tag{5}$$

$$u' = u - \langle u \rangle, \tag{6}$$

where the N is the number of available wave groups and T is the wave period. $\langle u \rangle$ contains the mean and periodic components of the velocity. The concept of the phase-averaged method is illustrated in Fig. 2 with the horizontal velocity u as an example.

In this study, the raw time-series velocity data were first filtered to remove poor-quality data (beam correlations <70 % and signal-to-noise ratios <12), then despiked by the moving average method (Cheung and Street, 1988; Su et al., 2015). Subsequently, the velocity data were divided into 70 individual waves by up-crossing method. Following Olfateh et al. (2017), these individual waves were categorized into 14 packets, with each packet containing 5 individual waves. Next, these individual waves in each packet were overlapped together and decomposed into an average component (stable part) and a fluctuated component (turbulence part). Finally, the turbulence parts of these packets were averaged, and the ensemble standard deviations were calculated.

Regarding the energy spectrum method, the turbulent velocity (e.g., in the horizontal direction) can be identified based on the inertial subrange of the energy spectrum. Fig. 3 depicts an example of the energy spectrum on wind-only conditions with $U_0 = 6$m s^{-1}. Fig. 3 suggests that no significant peak appears under wind-only conditions. This implies that the effect of wind on water turbulence is mainly through the wind-induced flow, under the present experimental settings. The turbulence spectrum can be identified by the part of high frequency which follows the trend of $f^{-5/3}$ in Fig. 3.

After extraction of the turbulence component from raw velocity data, several representative turbulence parameters were calculated. The horizontal and vertical turbulence intensities (σ_u and σ_w) reflect the variation of the turbulence and greatly influence the sediment transport and the near-bottom sediment concentration in the surf zone (Ting and Kirby, 1994). The horizontal and vertical turbulence intensities, σ_u and σ_w, can be calculated as follows:

$$\sigma_u = \sqrt{\overline{u'^2}} \tag{7}$$

Table 2
Summary of experiment settings. The capital letter A-D represent wave heights H = 6 cm, 8 cm,10 cm, 12 cm, respectively; the numbers represent different wind speed cases.

H(cm)				U_0(m s^{-1})	h (cm)	T (s)
6	8	10	12			
A0	B0	C0	D0	0	30	1.5
A1	B1	C1	D1	1.5		
A2	B2	C2	D2	2.5		
A3	B3	C3	D3	3.5		
A4	B4	C4	D4	6		

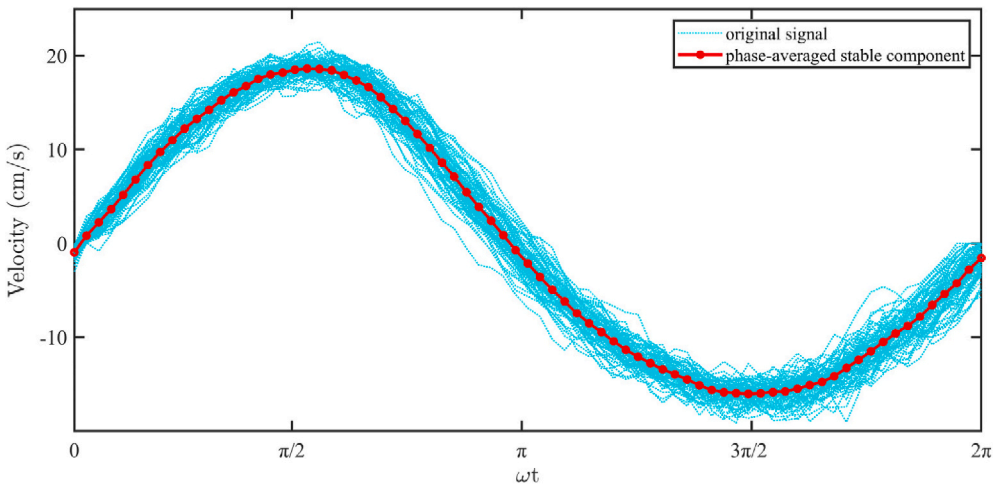

Fig. 2. The decomposition of the velocity into stable components and turbulence components.

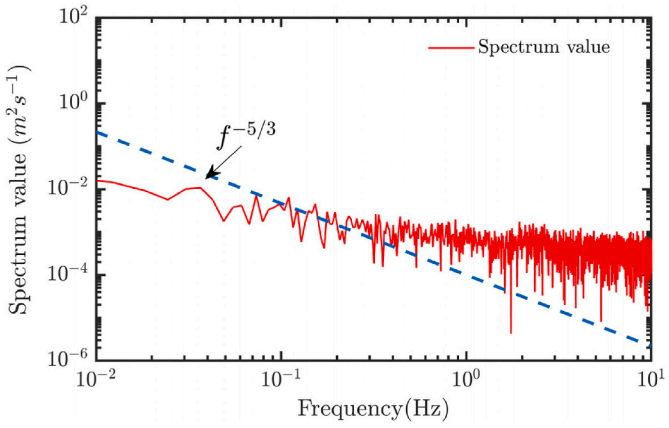

Fig. 3. Example of energy spectrum on wind-only condition (U_0 = 6 m s^{-1}).

$$\sigma_w = \sqrt{\overline{w'^2}} \tag{8}$$

The *TKE* of the water column, which represents the fluctuation degree of the turbulence velocity, is calculated from the decomposed turbulence component in three directions (longitudinal, vertical, and lateral) according to:

$$TKE = 1/2\left(\overline{u'^2} + \overline{w'^2} + \overline{v'^2}\right) \tag{9}$$

Subsequently, the turbulence structure of the water column is investigated by analyzing both the time-averaged and phase-averaged distribution of the turbulence parameters mentioned above.

4. Results

4.1. Time-averaged velocity profiles

Fig. 4 shows the vertical distribution of time-averaged velocity profiles of experimental cases A to D. Note that, the highest velocity

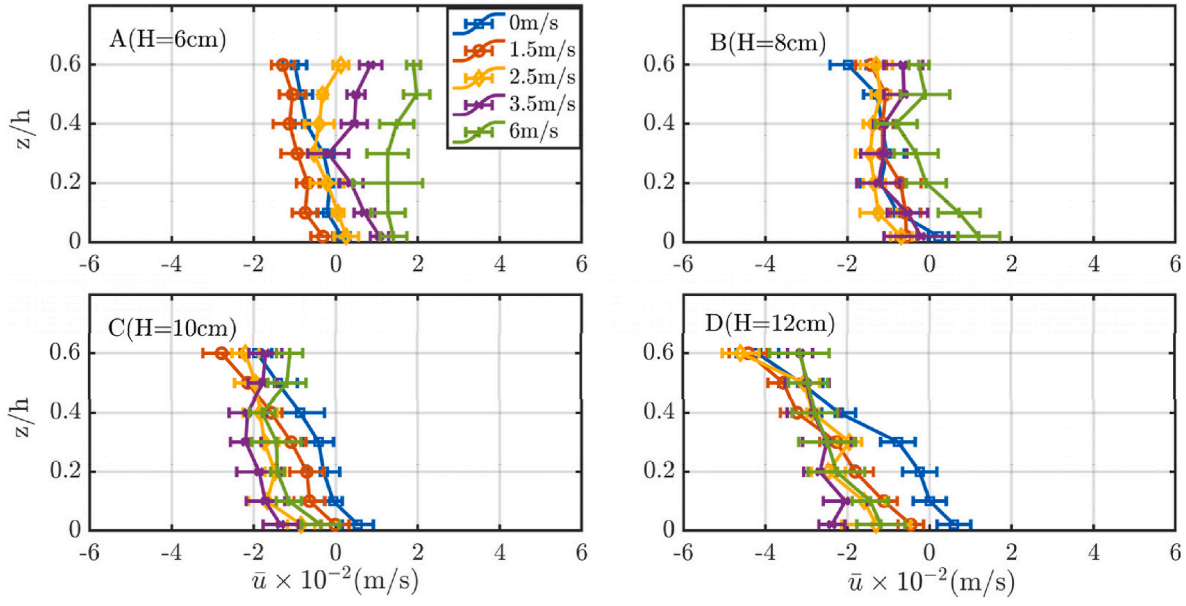

Fig. 4. The average velocity profiles as a function of normalized height. Lines of different colors represent waves combined with wind of various strengths. The capital letters at the upper left in each graph represent the experimental run and the number in the bracket represents the corresponding wave height. Bars are ensemble standard deviations.

measurement point is positioned at 0.6h above the bottom. Most velocities show negative values, which are consistent with the wave-induced flow velocity profile as well as the wind-induced flow profile in the middle and lower water layers (Longuet-Higgins, 1953; Longo et al., 2012). Only for one experiment in Group A (with 6 cm of wave height and 6 m s^{-1} of wind speed), the mean velocity profile is positive in lower water layers. This deviation may be a result of nonlinear interactions between a specific wave-wind combination, which requires further investigation.

Compared with the wave-only case (blue lines), the impact of the stronger wind (≥3.5 m s^{-1}) remarkably interferes with the average velocity profiles in each case. Taking case C (Fig. 4c) for example, the shape of the average velocity has changed little under a relatively gentle wind (1.5 m s^{-1}), and the average velocity of the middle water layer in C2-C4 gradually changes in the opposite direction (*x*-axis positive) as the wind becomes stronger, causing the average velocity profiles to be vertically more homogenous. This is a transformation from Stokes' drift under wave-only conditions into a wind-induced circulation.

4.2. Variations of wave parameters

Fig. 5a and b shows the time-series water surface elevations of Case A and C, respectively. The wave shape has little change under relatively small wind (e.g., A2 and C2), while it displays obvious high skewness with a short and high wave crest and a long and flat wave trough in Case A4 and C4. In order to describe the wave shape quantitatively, the wave asymmetry (*As*) and skewness (*Sk*) were estimated as follows (Feddersen and Veron, 2005; Grasso et al., 2012; Sous et al., 2021):

$$Sk = \frac{\langle (\eta - \langle \eta \rangle)^3 \rangle}{\langle (\eta - \langle \eta \rangle)^2 \rangle^{3/2}}, \tag{10}$$

$$As = \frac{\langle HT^3 (\eta - \langle \eta \rangle) \rangle}{\langle (\eta - \langle \eta \rangle)^2 \rangle^{3/2}}, \tag{11}$$

where η is the water surface elevations measured by the four wave gauges, *HT* is the Hilbert transformation and $<\cdot>$ represents the average operator. We calculated the wave skewness (*Sk*) and asymmetry (*As*) parameters for four wave gauges respectively, and the results have been averaged as shown in Fig. 5. The *Sk* (Fig. 5c) is increased with the wave height under wave-only conditions, as the wind superimposed, the *Sk* increased with wind speed proportionally and the relatively strong wind (i.e., $U_0 = 6 m s^{-1}$) leads to significant increment in *Sk,* which can be well verified by the wave shape in Fig. 5a. The wave shape has little changed under relatively small wind (A2) while it displays obvious high skewness with a short and high wave crest and a long and flat wave trough in Case A4. This phenomenon is consistent with the research of Zdyrski and Feddersen (2022) that the onshore wind has a strong impact on

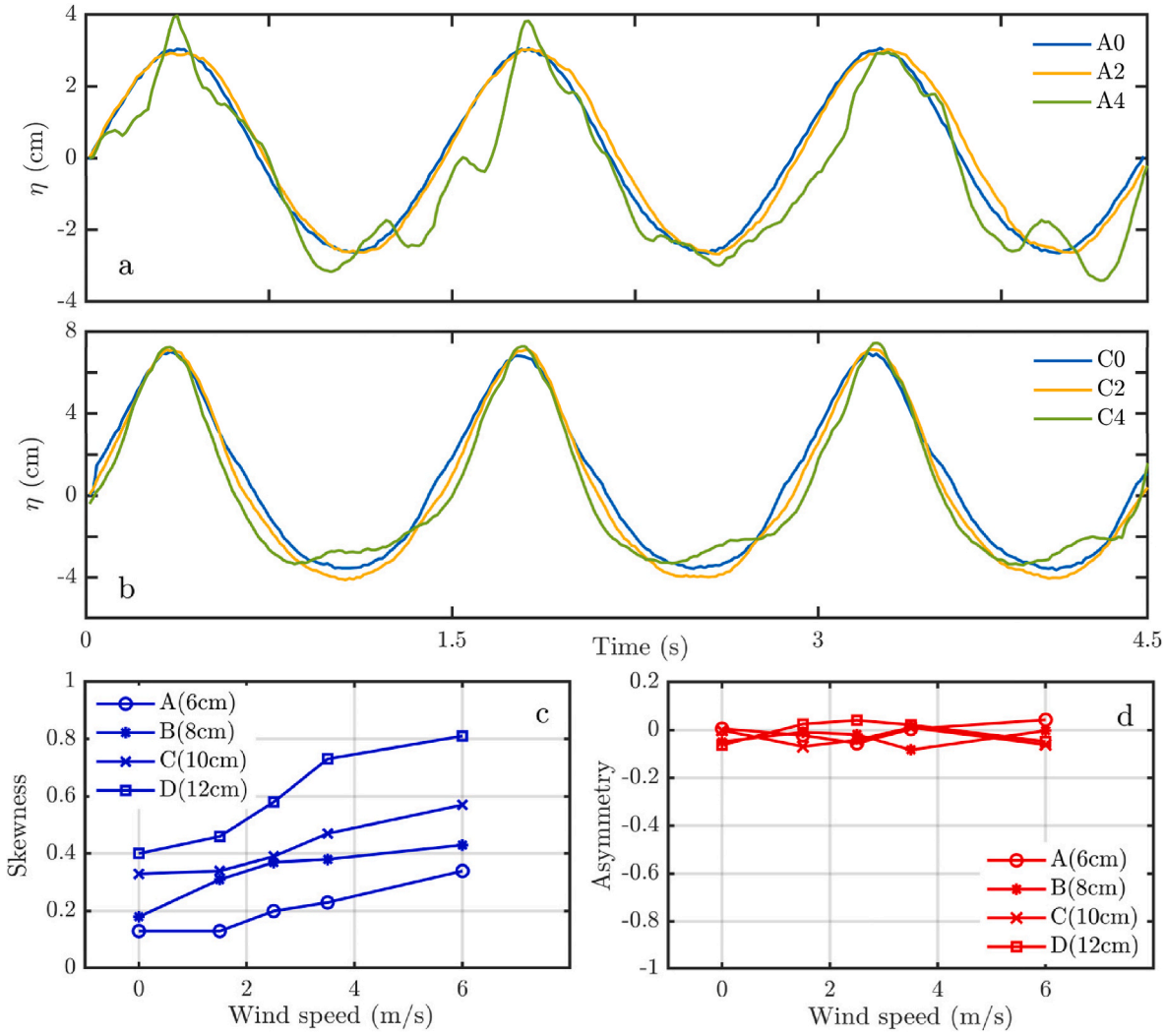

Fig. 5. Wave shapes of each condition. (a) and (b) are part of the time-series water surface elevations of Case A and C, respectively (i.e., $U_0 = 0 m s^{-1}$, 2.5 m s^{-1}, 6m s^{-1}). (c) and (d) are the wave skewness (Sk) and asymmetry (As), respectively.

narrowing the wave peak. However, the *As* (Fig. 5d) shows little change during various wave and wind conditions with the values fluctuating around 0, and the according results can be seen clearly in the wave shape (Fig. 5a). Although under the stronger wind in A4 (i.e., 6m s^{-1}), the wave asymmetry is not so remarkable.

Fig. 6 depicts variations in the mean wave height of all experimental cases. Under conditions where the paddle wave height is less than 8 cm, the wave height indeed increases when the wind speed increases to 6 m s^{-1}. When the wave height is larger than 10 cm, there is no significant increase in the mean wave height. Besides, the maximum near-bed orbital velocities, shown in Fig. 7, are also calculated based on velocity data at 0.6 cm above the bed. The maximum near-bed velocities stayed almost at a constant value under different wind-wave conditions. Thus, additional wind has little influence on the near-bed velocity. This indicates that near-bed velocities are controlled by a wave boundary layer generated by the paddle waves. Hence, the impact of the wind can hardly be extended to the wave boundary layer.

4.3. Variations of $\overline{uw}$, $\overline{\tilde{u}\tilde{w}}$ and $\overline{u'w'}$

For enclosed systems such as the laboratory flume in this study, lakes and semi-enclosed systems, such as tidal flat areas, the return flows can be generated to satisfy the conservation of mass due to the blocking effect of the closed end. As described in Eq. [1] and [2], time averages of the decomposed components $\overline{uw}$, $\overline{\tilde{u}\tilde{w}}$, $\overline{u'w'}$ (case A and C), which represent secondary circulation, wave-induced Reynolds stress and turbulent Reynolds stress, respectively, are shown in Fig. 8. Note that, these velocity terms are scaled with respect to H^2T^{-2}, where T is the wave period and H is the wave height, following Addona et al. (2018).

In general, the wave-induced Reynolds stress $\overline{\tilde{u}\tilde{w}}$, an order of magnitude larger than $\overline{uw}$ and two orders of magnitude larger than $\overline{u'w'}$, is exhibiting a dominant role in wave motions in shallow waters. By the normalization of the $\overline{\tilde{u}\tilde{w}}$ with H^2T^{-2}, the wave-induced Reynolds stress in this study (i.e., high-intensity wave) is consistent with previous studies with relatively moderate wave conditions (e.g., Olfateh et al., 2017; Addona et al., 2018, 2023).

The $\overline{uw}$ profiles of both case A and case C show an increase in response to the growing wind, and the wind effect on the profile alternation with larger wave height (case C with $H = 10$ cm) is relatively small. Under the relatively small wave height condition (i.e., $H = 6$ cm), the variation trend of the $\overline{uw}$ profiles with increasing wind speeds are consistent with Olfateh et al. (2017); however, an opposite trend emerges with large wave heights (i.e., $H = 10$ cm). This may be due to the relative strength between mechanically generated surface wave and wind, which will be discussed in Section 4. For $\overline{\tilde{u}\tilde{w}}$, the wind effect on $\overline{\tilde{u}\tilde{w}}$, appears less considerable under larger wave height (Case C) as well. Similar phenomena appear also for $\overline{u'w'}$ profiles. The $\overline{u'w'}$ are evenly distributed with minor values of around 0 in wave-only and gentle wind conditions (1.5 m s^{-1}, 2.5 m s^{-1}). As the wind becomes stronger one or two obvious peaks can be observed. For example, a sudden increase appears at $z/h = 0.5$ of every wind condition for case A. This indicates that enhanced wave intensity suppresses the turbulent momentum flux from surface winds to propagating waves.

4.4. Turbulence intensity and turbulence kinetic energy (TKE)

Fig. 9 displays the time-averaged horizontal turbulence intensities σ_u, the vertical turbulence intensities σ_w and *TKE* (normalized by H^2T^{-2}), taking case A and case C as examples.

Compared to case A0 (wave-only condition), the σ_u increases noticeably in case A1 (1.5 m s^{-1}) and A2 (2.5 m s^{-1}) with little difference between each other, and then σ_u continues to grow as the wind speed increases. When the wind increases to 6 m s-1, the σ_u of each layer increases noticeably. The variation pattern of σ_u profile in case C is almost the same as in case A. However, the wind influence on σ_u declined as the wave height increased, which is the same as that in Fig. 8. Note that the increased amplitude of σ_u, both in cases A and C, gradually decreases along the water depth, which indicates that the wind-induced energy transfers downward with attenuation. The variations of σ_w and *TKE* show almost the same trend with σ_u. The difference is that the values of σ_w are generally smaller that σ_u and the shape of the profile becomes steeper along the water column.

4.5. Time-averaged wind contribution on turbulence intensity

By comparing the results of the wave-only, wind-only and wind-wave experiments, we can identify the wave-induced, wind-induced and wind-wave-interaction contribution to water turbulence respec-

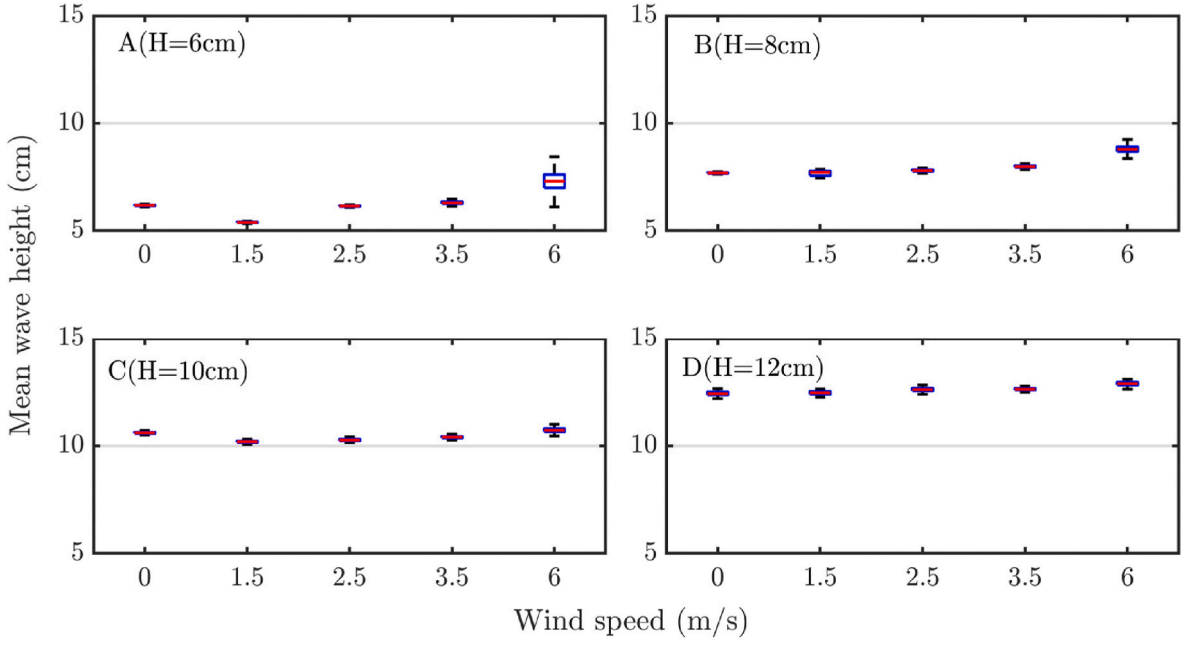

Fig. 6. Variations of mean wave height of different experimental cases. The capital letters at the upper left in each graph represent the wave height of each case.

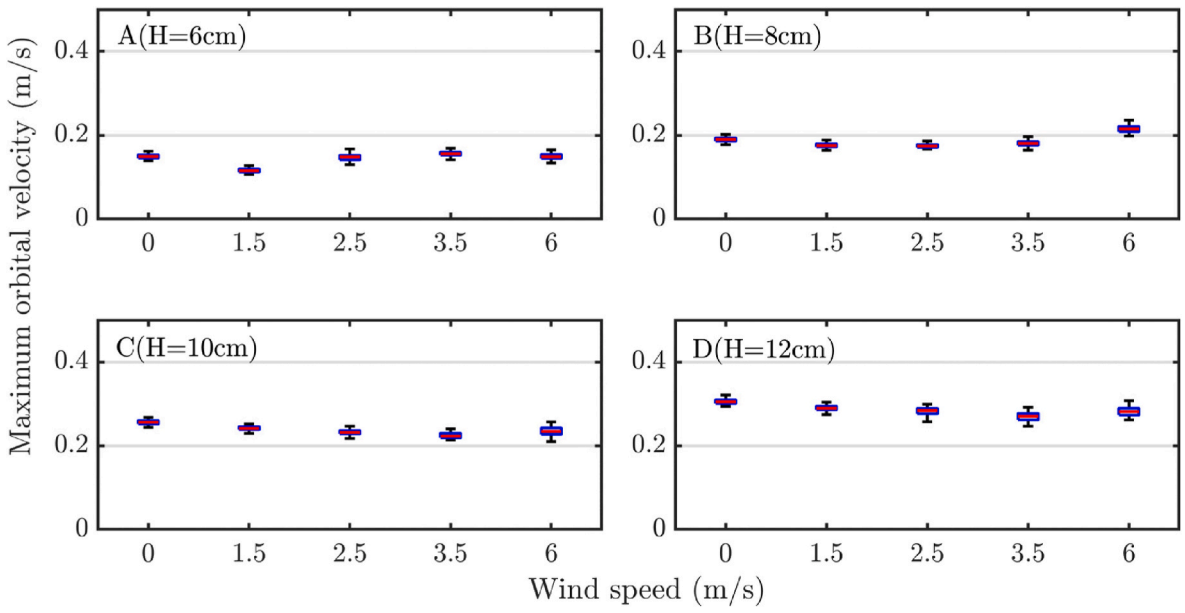

Fig. 7. The maximum orbital velocity of all experimental cases. The capital letters at upper left in each graph represent the wave height of each case.

tively, by assuming a linear superposition of the above three components. Thus, the wind-induced contribution to turbulence intensities can be calculated by comparing wind-only and wind-wave experiments:

$$\beta_u(z) = \frac{\sigma_{u-wi}(z)}{\sigma_{u-ww}(z)} \times 100\% \tag{12}$$

$$\beta_w(z) = \frac{\sigma_{w-wi}(z)}{\sigma_{w-ww}(z)} \times 100\% \tag{13}$$

The wave-induced contribution can be calculated by comparing wave-only and wind-wave experiments:

$$\alpha_u(z) = \frac{\sigma_{u-wa}(z)}{\sigma_{u-ww}(z)} \times 100\% \tag{14}$$

$$\alpha_w(z) = \frac{\sigma_{w-wa}(z)}{\sigma_{w-ww}(z)} \times 100\% \tag{15}$$

The wind-wave-interaction contribution can be calculated as follows:

$$\gamma_u(z) = \frac{\sigma_{u-ww}(z) - \sigma_{u-wa}(z) - \sigma_{u-wi}(z)}{\sigma_{u-ww}(z)} \times 100\% = 1 - \alpha_u(z) - \beta_u(z) \tag{16}$$

$$\gamma_w(z) = \frac{\sigma_{w-ww}(z) - \sigma_{w-wa}(z) - \sigma_{w-wi}(z)}{\sigma_{w-ww}(z)} \times 100\% = 1 - \alpha_w(z) - \beta_w(z) \tag{17}$$

in which, $\sigma_{u-wi}(z)$, $\sigma_{u-wa}(z)$ and $\sigma_{u-ww}(z)$ are the time-averaged horizontal turbulence intensities of wind-only, wave-only and wind-wave combined conditions respectively; $\sigma_{w-wi}(z)$, $\sigma_{w-wa}(z)$ and $\sigma_{w-ww}(z)$ are the time-averaged vertical turbulence intensities of wind-only, wave-only and wind-wave combined conditions respectively.

Fig. 10 depicts the vertical distributions of β_u and β_w (wind-induced contribution) as well as γ_u and γ_w (wind-wave-interaction contribution) in each experimental condition. Regarding wind-induced contributions, the β_u in each wind condition is relatively stable throughout the water depth and slightly increases when the wind becomes stronger (Fig. 10a), while β_w follows the same trend but the variations are more distinguishable (Fig. 10c). Regarding contributions of wind and wave interactions, γ_u and γ_w shows some differences in contrast to β_u and β_w. The γ_u of each wind condition drops suddenly to a rather low level (less than 18 %) below $z/h = 0.3$, while they are relatively stable above this height (Fig. 10b). In each wind condition, γ_w displays a growing trend in a downward direction, reaching the maximum at $z/h = 0.2$, and then decreases (Fig. 10d). Besides, there are little differences of γ_w in each condition, indicating that a relatively stable γ_w is independent of wind and wave conditions.

Fig. 11 displays the depth-averaged values of the total wind contribution to σ_u ($\delta_u = \beta_u + \gamma_u$) and σ_w ($\delta_w = \beta_w + \gamma_w$) versus wave height and wind speed. Both δ_u and δ_w are basically proportional to the wind speed in each case. One noticeable observation is that δ_u and δ_w of case A (smaller wave height, 6 cm) are the largest in all wind conditions, while in case D, δ_u and δ_w are the lowest. This demonstrates that the wave effect, as in case D, overrules the wind and plays a dominant role in the contribution to the turbulence intensities (δ_u and δ_w) of the whole water column. Besides, the total value of δ_w is larger than δ_u, revealing that σ_w is more sensitive to the additional wind than σ_u, and that the turbulence brought by the additional wind tends to transfer downward along the water depth, intervening with the vertical turbulence intensity σ_w.

4.6. Wind contribution on turbulence intensity at different wave phases

As mentioned before, by using the phase-average method, we can extract the turbulence parameters (e.g., turbulence intensity) at different wave phases. From the phase-averaged turbulence intensity obtained under wind-wave conditions, by subtracting the values obtained under wave-only conditions, we can analyze the impact of the wind at different phases. Thus, the wind contribution to turbulence intensity (r_u for horizontal and r_w for vertical) at different wave phases is defined as:

$$r_u = \frac{\widetilde{\sigma}_{u-ww}(z) - \widetilde{\sigma}_{u-wa}(z)}{\widetilde{\sigma}_{u-ww}(z)} \times 100\% \tag{18}$$

$$r_w = \frac{\widetilde{\sigma}_{w-ww}(z) - \widetilde{\sigma}_{w-wa}(z)}{\widetilde{\sigma}_{w-ww}(z)} \times 100\% \tag{19}$$

in which, $\widetilde{\sigma}_{u-wa}(z)$ and $\widetilde{\sigma}_{u-ww}(z)$ are the horizontal turbulence intensities of wave-only and wind-wave combined conditions at different wave phases respectively; $\widetilde{\sigma}_{w-wa}(z)$ and $\widetilde{\sigma}_{w-ww}(z)$ are the vertical turbulence intensities of wave-only and wind-wave combined conditions at different wave phases respectively. Note that, r_u and r_w include the both wind-only effect and the wind-wave interaction effect on turbulence intensity.

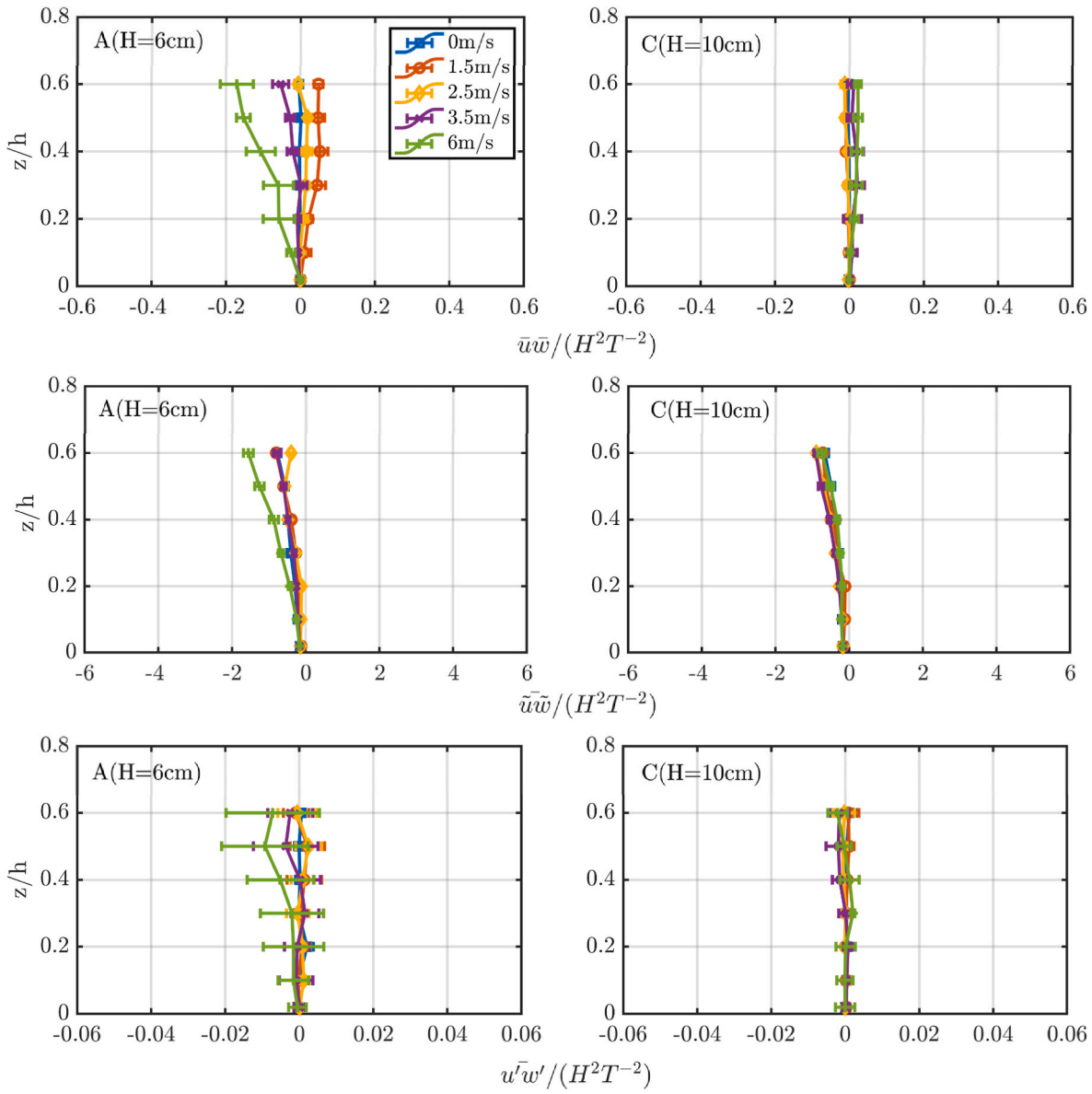

Fig. 8. Time-averaged $\overline{uw}$ (upper), $\overline{\tilde{u}\tilde{w}}$ (middle), $\overline{u'w'}$ (bottom) as a function of normalized height. Lines of different colors represent waves combined with wind of various strengths. The capital letters at upper left in each graph represent the wave height. Bars are ensemble standard deviations.

Similarly, as in the previous time-averaged results, r_u at the same vertical position increases with a stronger wind speed, while r_u decreases in the downward direction in each condition (Fig. 12). The maxima mainly appear at $\pi/2$-$3\pi/2$ at the middle layer ($z/h = 0.6$) and the lower layer ($z/h = 0.3$), although the differences are not obvious among the four phases. However, for r_u at the bottom layers ($z/h = 0.02$), there are two peaks around $\pi/2$ and $3\pi/2$, respectively, in each wind condition. With respect to r_w (Fig. 13) compared to σ_u, two differences can be observed. Firstly, the disparities between phases are very small in each layer and no remarkable peaks exist within a wave period. Secondly, in general, the r_w shows an increased trend in the downward direction from the water surface to the bottom, which is consistent with Fig. 10.

5. Discussions

5.1. Reliability of turbulence separation

The practicability of phase-average has been discussed in extensive research works, for example, one of its advantages is that it does not assume linearity or potential behavior for the wave-related motion (Thais and Magnaudet, 1996), so the turbulence component u' can be define as the non-periodic part of the velocity (Eq. (6)). On the other hand, the filtering process can be problematic since it is the superposition of the generated regular wave from wave maker in the laboratory and the short random wave from the wind. Qiao et al. (2016) reported that the phase-average method can be applicable and reliable in condition of mechanically generated waves under a relatively light wind after discussing the separating approaches of many investigators, by taking the work of Thais and Magnaudet (1996) as an example (wave height = 3–4.2 cm, wind speed = 0–5.8 m s^{-1}). Similar research has been done by Cheung and Street (1988) (wave height 4.1–4.4 cm, wind speed = 1.7–6.2 m s^{-1}), whose experimental setups were quite similar to the present study. Herein, we made a comparison of the horizontal turbulence intensity σ_u ($\sqrt{\overline{u'^2}}$) between the results of Cheung and Street (1988) and the present study (Run A) in Fig. 14. It shows that the horizontal intensities of the two studies are of the same magnitude and the variation pattern along water depth and similar comparison and

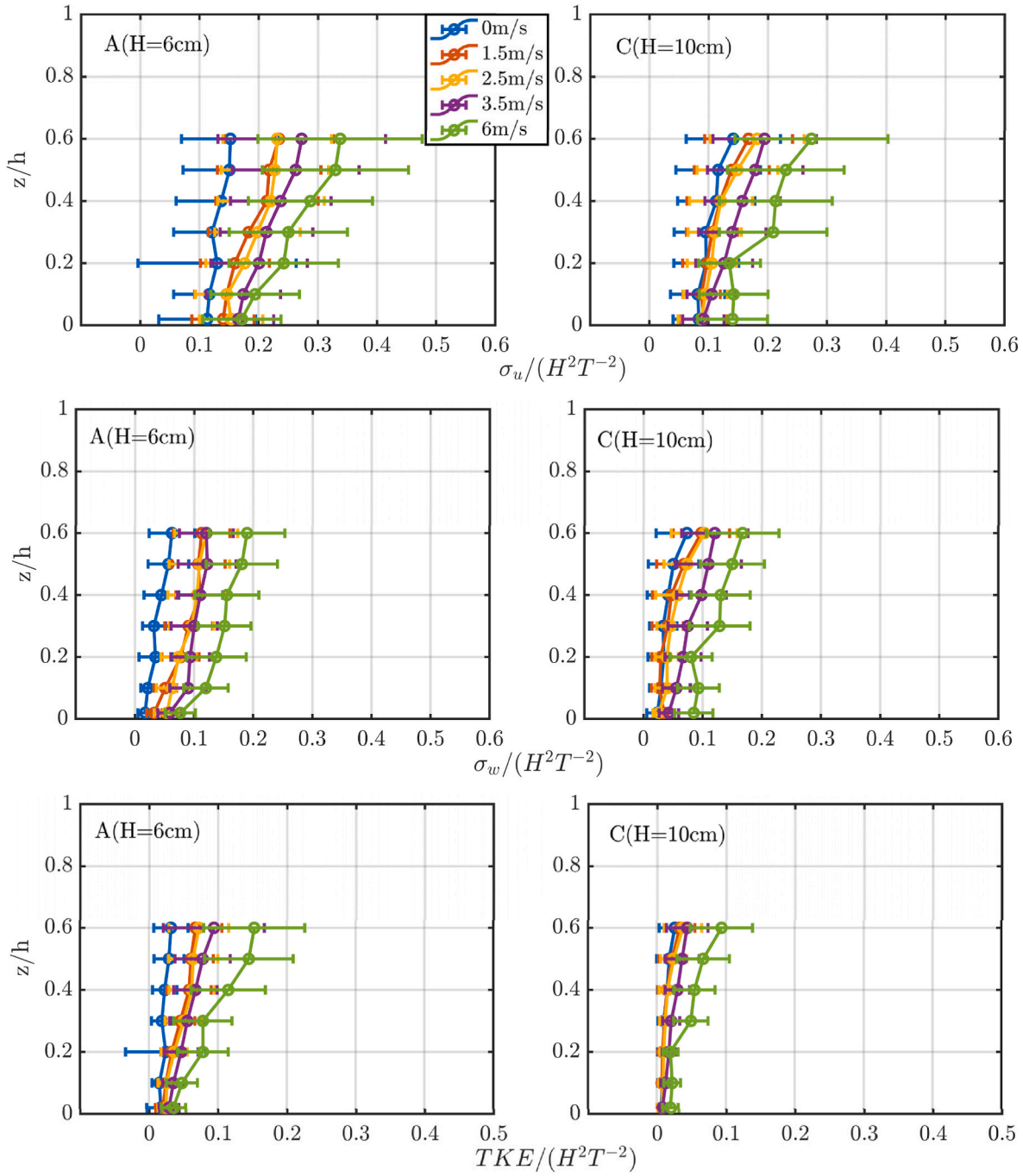

Fig. 9. Time-averaged σ_u (upper), σ_w (middle), *TKE* (bottom) as a function of normalized height. Lines of different colors represent waves combined with wind of various strengths. The capital letters at the upper left in each graph represent the wave height of each case. Bars are ensemble standard deviations.

accordant results can be found in Thais and Magnaudet (1996) and Wei et al. (2018), so the practicability and reliability of phase-average to the present wind and wave data are manifested. Additionally, one remarkable advantage of the phase-average method for the present study is that the wind effect extent and mechanism among wave phases within a wave period can also be explored.

During the experimental data process, two methods were chosen for the water turbulence decomposition under different experimental conditions. The energy spectrum analysis method was used for the wind-only conditions while for the wave-only and wind-wave combined conditions, the phase-average method was applied. Therefore, it is necessary to compare the turbulence separation results by these two methods to ensure the data validity. Taking the velocity measurements of Run C as examples, the horizontal turbulence intensity σ_u was computed by the energy spectrum method and compared with the result of the phase-average. Fig. 15 shows an example of the energy spectrum of C3 (wave height of 10 cm and wind speed of 3.5 m s^{-1}). Table 3 displays the quantitative comparison between the two methods. The depth-average deviations between the two methods are 4.6 %–10.9 % and the deviations increase with increased wind speed. This result shows that the differences in this study are reasonable and the turbulence estimations are reliable.

5.2. Additional impact of wind on water waves

In this study, we examined the contributions of additional wind-

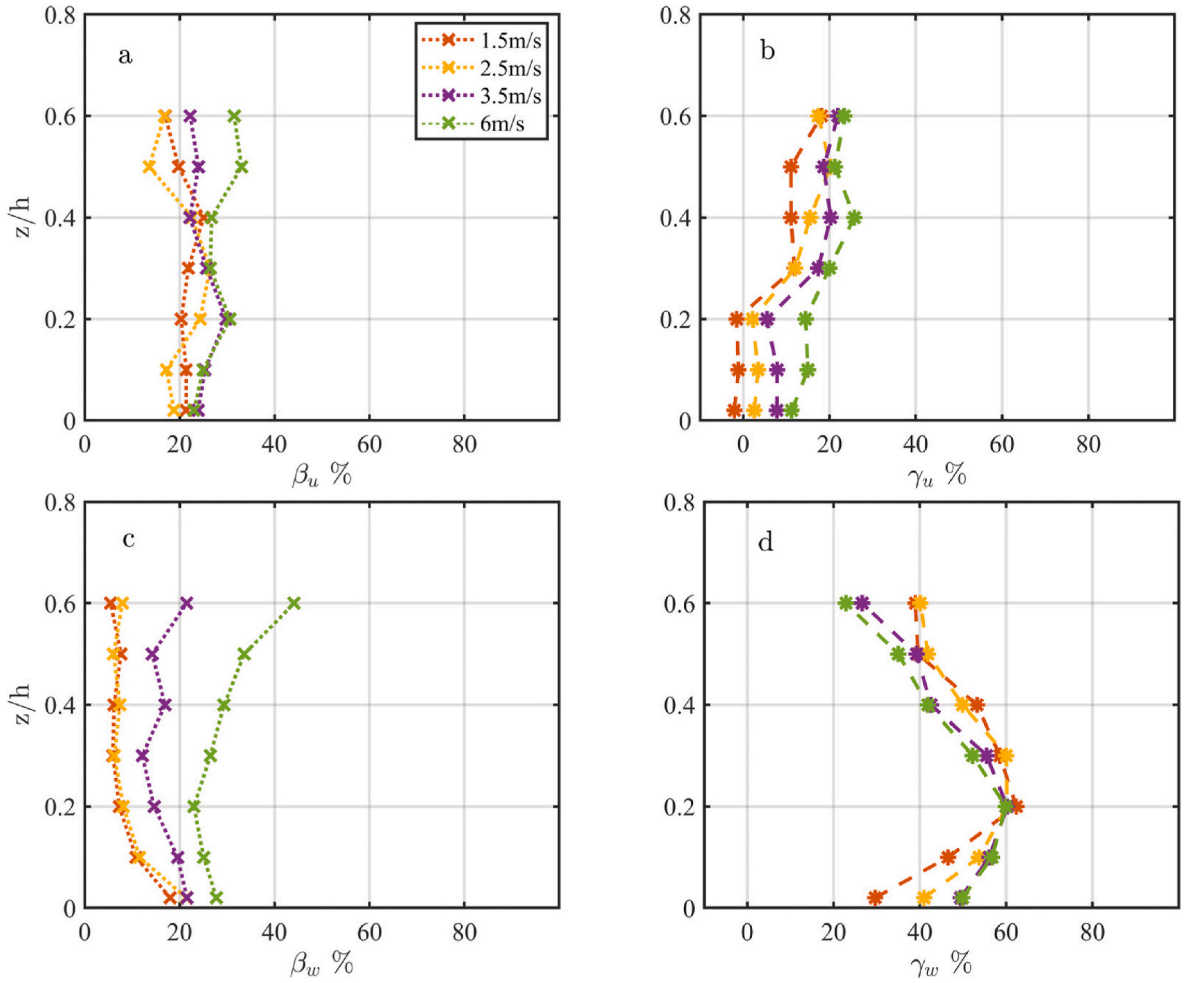

Fig. 10. Time-average of wind-only (cross line left, subplots a and c) and wind-wave interaction (dash line right, subplots b and d) contribution to σ_u and σ_w as a function of normalized height. Lines of different colors represent various wind speed conditions.

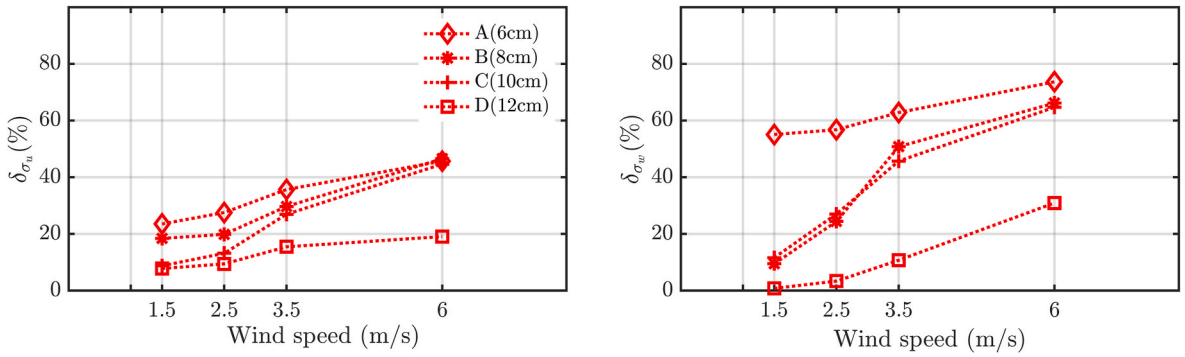

Fig. 11. Depth-averaged values of turbulence intensities wind contribution ratio δ_u and δ_w.

induced momentum in water in addition to wave-induced momentum, by a series of experiments in a wind-wave flume. Hydrodynamic features under various combinations of waves and winds were investigated with respect to shallow waters. The results have shown that wind can introduce additional complexities compared to wave-only conditions in different scales. In the macroscopic aspect, the wave skewness was distorted to a larger degree than wave asymmetry by additional winds. The stronger the wind speed, the larger the magnitude of wave skewness. This is according to the existing study that an increasing difference between the wave crest and trough shape will be evident under the condition of the wave with wind superposed (Addona et al., 2018). Under wave-only conditions, a time-average velocity profile suggests the feature of a bottom layer toward the onshore and an upper layer toward the offshore (Fig. 4). With the additional wind, the velocity profile of a wave-only condition was changed to a more homogenously distributed shape. This is due to the secondary circulation by wind in a closed or semi-closed area. However, this circulation can be modulated by surface waves: a larger wave-induced velocity profile is less affected by this wind-induced circulation. Furthermore, near bed boundary layer dynamics were still dominated by the paddle wave, because the orbital

Fig. 12. Averaged phase-distribution of r_u of the three layers of the water column in a wave period. The numbers in each graph represent the average values of r_u within each phase.

velocities under different wind conditions were similar to a wave-only case.

In shallow waters, the wave-induced Reynolds stress $\overline{\tilde{u}\tilde{w}}$, an order of magnitude larger than $\overline{uw}$ and two orders of magnitude larger than $\overline{u'w'}$, is exhibiting a dominant role in wave motions in shallow waters. The $\overline{uw}$ and $\overline{u'w'}$ are in the same order of magnitude as the results of the previous observations in shallow water systems (Olfateh et al., 2017), whereas the $\overline{\tilde{u}\tilde{w}}$ is an order of magnitude larger (Fig. 8). This is due to the larger relative wave height used in the present study representing features of shallow waters, especially during rough weather. With respect to additional wind effects on $\overline{\tilde{u}\tilde{w}}$, it is found that only stronger wind (i.e., 6m s^{-1}) can increase $\overline{\tilde{u}\tilde{w}}$ in the upper layer. Yet, with the increase in wave height, the influence of wind is reduced. This again implies that wave motions are the major agency of wind energy transfer to water. However, in terms of turbulence structures, the present experimental study illustrates that wind can increase turbulence intensities compared to paddle wave-only cases in shallow waters. The increase of turbulence intensity is proportional to the wind speed, and decreases from the water surface to the bottom.

5.3. Wind effect on water turbulence

As mentioned before, wind can not only affect the water turbulence structure by wave motion (i.e., wave-induced turbulence) but can also directly exert turbulence on a water surface and then transfer downward (i.e., wind-induced turbulence). We considered that the enhancement of turbulence intensity is partly due to the direct impact of wind, and partly

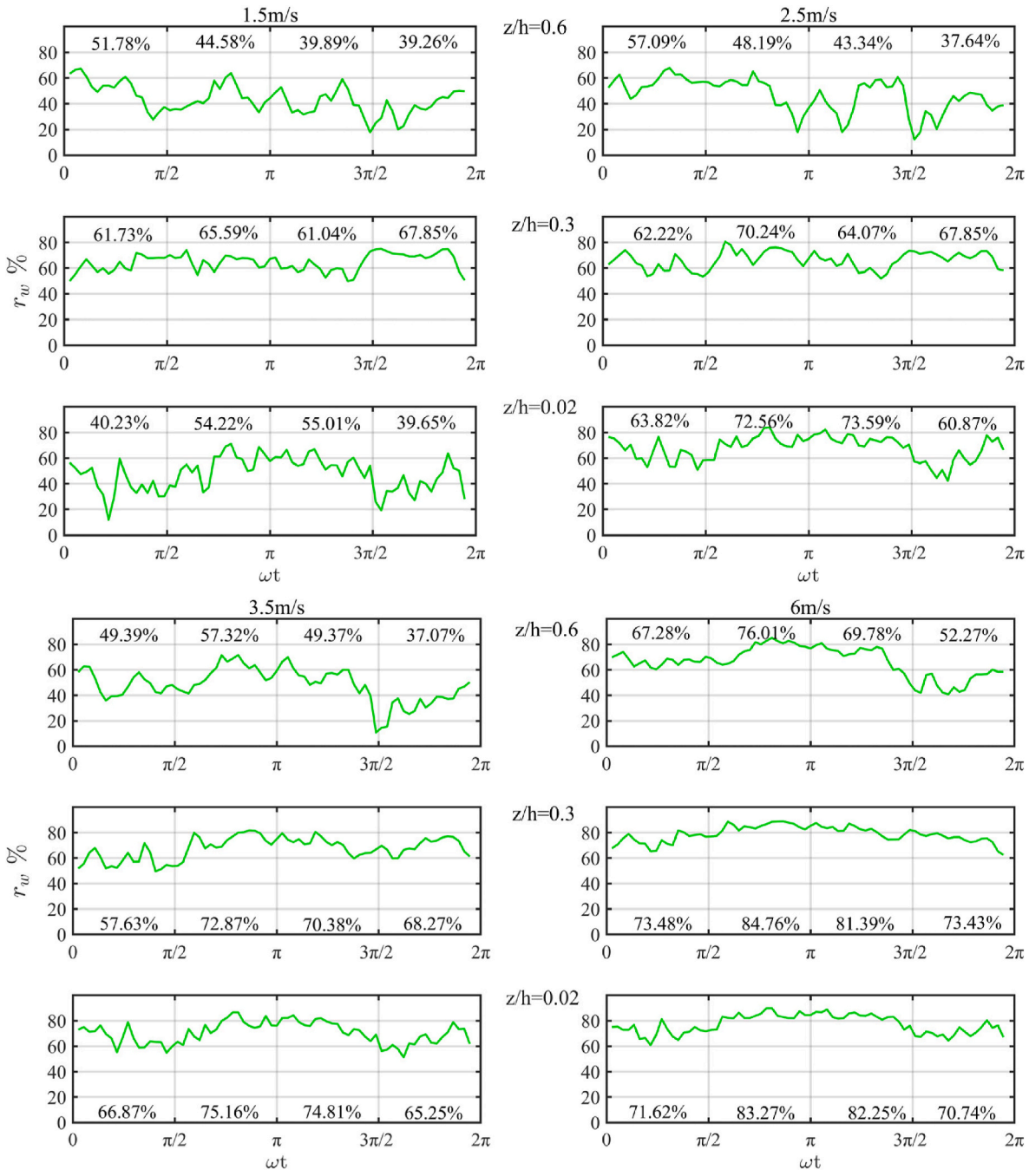

Fig. 13. Averaged phase-distribution of r_w of the three layers of the water column in a wave period. The numbers in each graph represent the average values of r_w within each phase.

through affecting the wave shape, which influences wave-induced turbulence. In most cases, these two turbulence incidents are generated simultaneously during windy weather, but only wave-induced turbulence is usually considered to result in mixing processes in the water column.

The results of the present study have shown that both horizontal (σ_u) and vertical turbulence intensities (σ_w) are enhanced with increased wind speed. The vertical turbulence intensity (σ_w) is found to be more sensitive to wind than the horizontal turbulence intensity (Fig. 8). The contribution of wind-induced turbulence can be as large as 70 % (Fig. 11), demonstrating that wind-induced turbulence is also important for vertical mixing processes in addition to waves. To explore the role of wind-induced turbulence on different wind and wave conditions, we further analyzed changes in the average wind-induced turbulence contribution against the ratio of wind speed to maximum near-bed orbital velocity of a paddle wave (hereafter referred to as relative wind strength; Fig. 16). Fig. 16 exhibits a monotonically increasing relationship (correlation coefficient of 0.976) between the contribution of wind-induced turbulence intensity and the relative wind strength. Linearly fitted results depict that wind dominates waves on vertical intensity, with a relative wind speed of over 25. This implies that in shallow waters, local wind-induced turbulence indeed plays a role in vertical mixing processes and the contribution of wind depends on the relative strength of local winds and offshore waves (e.g., swells).

Subsequently, the contributions of different turbulence sources (wave-only, wind-only, wind-wave interaction) can be separated by different experimental settings. Regarding vertical turbulence intensity, it is found that the role of wind-wave interaction is very prominent. The

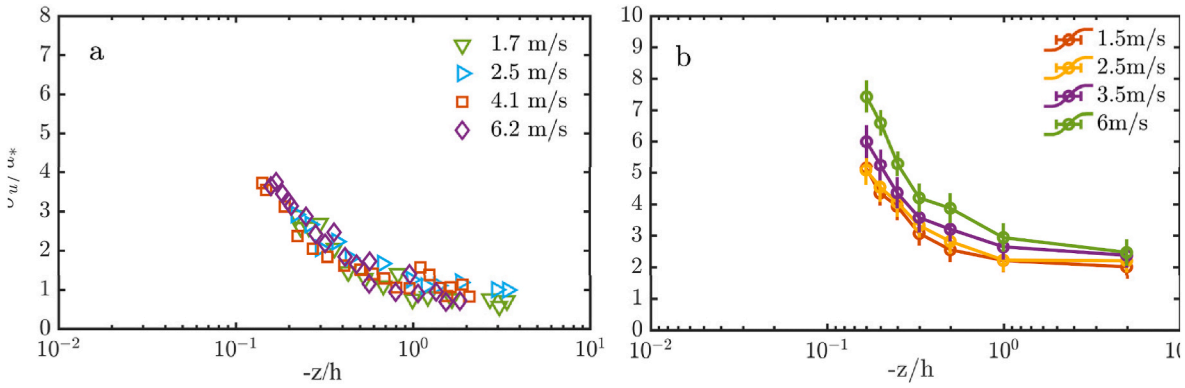

Fig. 14. The non-dimensional horizontal turbulence intensity versus the relative water depth. (a) Non-dimensional horizontal turbulence intensity of Cheung and Street (1988), (b) Non-dimensional horizontal turbulence intensity of present study.

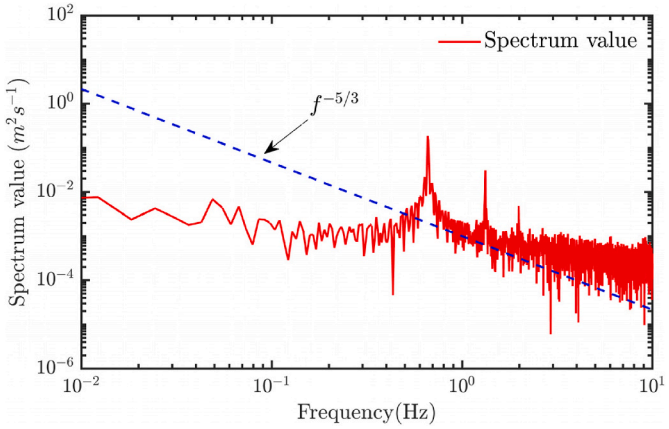

Fig. 15. The energy spectrum for turbulence decomposition of C3.

contribution ratio of wind-wave interaction (γ_w) on vertical turbulence intensity varies little with different wind speeds, depicting a peak value (around 60 %) at 0.2*h*, then decreasing upward and downward (Fig. 10d). This phenomenon indicates that when wind blows with surface waves, the major source of wind-induced turbulence is induced by a nonlinear wind-wave interaction, which reinforces vertical turbulence above the wave boundary layer. Furthermore, wind-induced turbulence is active in all phases of paddle waves for vertical turbulence intensity (Fig. 10), indicating a successive effect of wind-induced turbulence.

Addona et al. (2018) reported that the wind-wave combined conditions are an enhancement of the efficiency in energy and momentum transfer from the wind to water, by analyzing the turbulence features in the upper-middle water column with moderate wave conditions (i.e., *H/h* of 0.074–0.10 and bed shear stress of 0.09–0.16). We extended our analysis to examine the wind effect on turbulence intensity and *TKE*, especially for lower and bottom water columns with relatively strong wave conditions (i.e., *H/h* of 0.133–0.4 and bed shear stress of 0.26–0.52), discovering that wind-wave interactions contribute up to 60 % of vertical turbulence enhancement at 0.2h above the bed. During rough weather, a high sediment concentration layer can form near the bottom of silty tidal flats (Yao et al., 2015). An increase in vertical turbulence intensity may further enhance the vertical diffusion of suspended sediment in the water column, intensifying suspended sediment transport. Consequently, wind-induced enhancement of vertical turbulence can play a role in influencing suspended sediment dynamics, deserving further studies.

6. Conclusion

The present research investigated the additional influence of local wind on water turbulence structures in shallow waters without and with gravity waves. By a series of flume experiments (e.g., paddle-induced gravity waves only, wind-only, combinations of wind and wave), wind effects can be decomposed into different terms (e.g., wind-driven currents, wind waves, wind-induced turbulence), which are active on different spatial and temporal scales. This study focused on the contribution of additional wind-induced momentum terms in a water column in addition to waves. The following conclusions can be drawn.

(1) Stronger wind increases the magnitude of wave skewness, but the near-bed boundary layer dynamics are still under the control of the paddle-generated waves. The additional wind can change the time-averaged velocity profile of wave-only conditions, to a more homogenous distribution shape. The wave motion is the primary

Table 3
The error analysis for the σ_u calculated by energy spectrum analysis and phase-average respectively. σ_{up} (cm s-1) represents the σ_u calculated by phase-average while σ_{us} (cm s-1) represents σ_u calculated by energy spectrum analysis, and e_s (%) represents the errors relative to σ_{us}. The last number of each e_s column is the average of the corresponding e_s.

Run C	U_0 (m s-1)											
	1.5			2.5			3.5			6		
z/h	σ_{up}	σ_{us}	e_s	σ_{up}	σ_{us}	e_s	σ_{up}	σ_{us}	e_s	σ_{up}	σ_{us}	e_s
0.01	0.55	0.52	***5.2***	0.53	0.60	***11.9***	0.55	0.65	***15.7***	0.84	0.74	***14.1***
0.1	0.53	0.58	***8.6***	0.57	0.61	***6.9***	0.63	0.68	***7.1***	0.86	0.76	***12.5***
0.2	0.58	0.57	***2.6***	0.63	0.64	***10.3***	0.76	0.70	***8.3***	0.81	0.82	***9.1***
0.3	0.64	0.62	***2.4***	0.66	0.70	***5.4***	0.84	0.90	***6.5***	1.25	1.03	***21.0***
0.4	0.72	0.76	***5.7***	0.73	0.86	***15.6***	0.94	0.89	***6.0***	1.28	1.12	***14.4***
0.5	0.83	0.81	***3.1***	0.89	0.83	***7.6***	1.07	1.17	***8.2***	1.38	1.31	***5.6***
0.6	0.10	0.96	***4.8***	1.09	1.22	***10.3***	1.17	1.18	***15.6***	1.64	1.53	***7.4***
			4.6			***8.4***			***9.6***			***10.9***

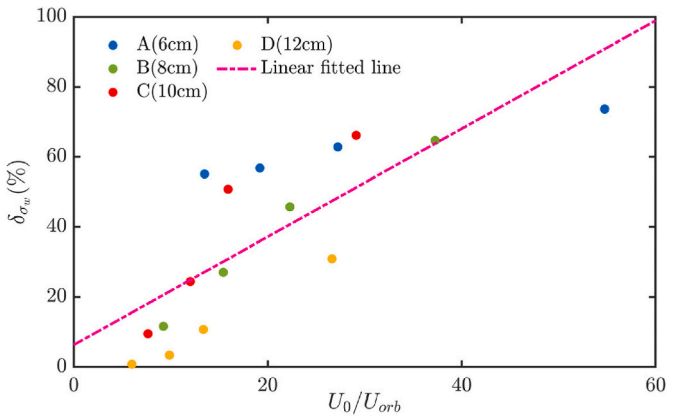

Fig. 16. Average wind-induced turbulence contribution versus the relative wind strength.

agency of the wind-introduced energy to waters, due to a leading role of wave-induced Reynolds stress factors $\widetilde{u}\widetilde{w}$ over $\overline{u'w'}$ and $\overline{uw}$ in shallow areas.

(2) More energy can be brought into the water column by stronger wind, enhancing the turbulent Reynolds stress $\overline{u'w'}$, horizontal and vertical intensities (σ_u and σ_w) and *TKE* in different degrees. The vertical intensities (σ_w) are more sensitive to the wind than σ_u, and the largest contribution of wind-induced turbulence to σ_w is over 70 %. Hence, the wind can directly influence water turbulence changing the vertical mixing processes in shallow waters.

(3) When wind blows with surface waves, the major source of water turbulence is induced by a nonlinear wind-wave interaction, especially for vertical turbulence intensities. The nonlinear wind-wave interaction accounts for up to 60 % of vertical turbulence intensities. This proportion on σ_w is relatively stable in each phase of waves. Further study is required to understand the relevant mechanism of nonlinear wind-wave interaction on turbulence enhancement.

In deep waters, downward momentum transport was affected by both wind and wave at a depth of approximately 0.75 times the dominant wavelength. However, the effect of the wave was diminished below this depth (e.g., Lin and Gad-el-Hak, 1984). For shallow water systems, this study found that both wind and wave can intervene the turbulence of whole water depth in shallow waters, which differs from that in deep waters. Therefore, more studies should be carried out to deepen the understanding on the impact of wind on the mixing processes of shallow waters.

CRediT authorship contribution statement

Peng Yao: Writing – review & editing, Writing – original draft, Methodology, Conceptualization. **Jinshan Pu:** Writing – review & editing, Writing – original draft, Visualization, Methodology, Formal analysis. **Yongping Chen:** Supervision, Formal analysis, Conceptualization. **Min Su:** Visualization, Investigation, Formal analysis. **Marcel J. F. Stive:** Writing – review & editing, Supervision, Methodology, Conceptualization. **Zhengbing Wang:** Writing – review & editing, Supervision, Formal analysis, Conceptualization.

Declaration of competing interest

The authors declare that they have no known competing financial interests or personal relationships that could have appeared to influence the work reported in this paper.

Acknowledgement

This work is funded by the National Key R&D Program of China (Grant No. 2023YFC3008100), the National Natural Science Foundation of China (Grant No. 42476166), the Fundamental Research Funds for the Central Universities (Grant No. B250201192), the National Natural Science Foundation of China (Grant No. 51620105005), and the Open Fund of Key Laboratory of Ocean Space Resource Management Technology, MNR, China (Grant No. KF-2023-106).

Data availability

Data will be made available on request.

References

Addona, F., Lira Loarca, A., Chiapponi, L., Losada, M.A., Longo, S., 2018. The Reynolds wave shear stress in partially reflected waves. Coast. Eng. 138, 220–226. https://doi.org/10.1016/j.coastaleng.2018.04.015.

Addona, F., Chiapponi, L., Clavero, M., Losada, M.A., Longo, S., 2020. On the interaction between partially-reflected waves and an opposing wind. Coast. Eng. 162, 103774. https://doi.org/10.1016/j.coastaleng.2020.103774.

Addona, F., Chiapponi, L., 2023. Velocity and stresses of partially-reflected water waves in the presence of opposing wind. Coast. Eng. 183, 104310. https://doi.org/10.1016/j.coastaleng.2023.104310.

Addona, F., 2024. Interaction between incident and reflected mechanical waves in the presence of an opposing wind. Coast. Eng. 193, 104572. https://doi.org/10.1016/j.coastaleng.2024.104572.

Agrawal, Y.C., Terray, E.A., Donelan, M.A., Hwang, P.A., Williams, A.J., Drennan, W.M., Kahma, K.K., Krtaigorodskii, S.A., 1992. Enhanced dissipation of kinetic energy beneath surface waves. Nature 359, 219–220. https://doi.org/10.1038/359219a0.

Ardhuin, Jenkins, 2006. On the interaction of surface waves and upper ocean turbulence. J. Phys. Oceanogr. 36 (1), 551–557. https://doi.org/10.1175/JPO2862.

Babanin, A.V., 2006. On a wave-induced turbulence and a wave-mixed upper ocean layer. Geophys. Res. Lett. 33. https://doi.org/10.1029/2006GL027308.

Benilov, A.Yu, Kouznetsov, O.A., Panin, G.N., 1974. On the analysis of wind wave-induced disturbances in the atmospheric turbulent surface layer. Boundary-Layer Meteorol. 6, 269–285. https://doi.org/10.1007/BF00232489.

Bliven, L.F., Huang, N.E., Long, S.R., 1984. A laboratory study of the velocity field below surface gravity waves. In: Brutsaert, W., Jirka, G.H. (Eds.), Gas Transfer at Water Surfaces. Springer, Netherlands, Dordrecht, pp. 181–190. https://doi.org/10.1007/978-94-017-1660-4_16.

Bosboom, J., Stive, M., 2021. Coastal Dynamics. Delft University of Technology.

Cavaleri, L., Zecchetto, S., 1987. Reynolds stresses under wind waves. J. Geophys. Res.: Oceans 92, 3894–3904. https://doi.org/10.1029/JC092iC04p03894.

Chávez-Dorado, J., Scherl, I., DiBenedetto, M., 2024. Wave and turbulence separation using dynamic mode decomposition. https://doi.org/10.48550/ARXIV.2403.00223.

Chen, Y., Pu, J., Zhu, Q., Su, M., Zhou, Z., Qiao, Z., Xu, C., Yao, P., 2023. Wind effect on sediment suspensions over silt-dominated mixtures: an experimental study. Front. Mar. Sci. 9, 1036381. https://doi.org/10.3389/fmars.2022.1036381.

Cheung, T.K., Street, R.L., 1988. The turbulent layer in the water at an air—water interface. J. Fluid Mech. 194, 133. https://doi.org/10.1017/S0022112088002927.

Dai, D., Qiao, F., Sulisz, W., Han, L., Babanin, A., 2010. An experiment on the nonbreaking surface-wave-induced vertical mixing. J. Phys. Oceanogr. 40 (1), 2180–2188. https://doi.org/10.1175/2010JPO4378.

Feddersen, F., Veron, F., 2005. Wind effects on shoaling wave shape. J. Phys. Oceanogr. 35, 1223–1228. https://doi.org/10.1175/JPO2753.1.

Feddersen, F., Trowbridge, J.H., Williams, A.J., 2007. Vertical structure of dissipation in the nearshore. J. Phys. Oceanogr. 37 (1), 1764–1777. https://doi.org/10.1175/JPO3098.

Feddersen, F., 2012. Scaling surf zone turbulence. Geophys. Res. Lett. 39. https://doi.org/10.1029/2012GL052970.

Fredsøe, J., Sumer, B.M., Kozakiewicz, A., Chua, L.H.C., Deigaard, R., 2003. Effect of externally generated turbulence on wave boundary layer. Coast. Eng. 49, 155–183. https://doi.org/10.1016/S0378-3839(03)00032-2.

Fujiwara, Y., 2024. Dynamics of turbulence production by attenuating interfacial gravity waves observed in air–water coupled wave-resolving simulation. J. Fluid Mech. 999, A97. https://doi.org/10.1017/jfm.2024.934.

Fulgosi, M., Lakehal, D., Banerjee, S., De Angelis, V., 2003. Direct numerical simulation of turbulence in a sheared airwater flow with a deformable interface. J. Fluid Mech. 482, 319–345. https://doi.org/10.1017/S0022112003004154.

Garett, C., Gemmrich, J., 2009. Rogue waves. Phys. Today 62, 62–63. https://doi.org/10.1063/1.3156339.

Gemmrich, J.R., Farmer, D.M., 2004. Near-surface turbulence in the presence of breaking waves. J. Phys. Oceanogr. 34, 1067–1086. https://doi.org/10.1175/1520-0485(2004)034<1067:NTITPO>2.0.CO;2.

Grasso, F., Castelle, B., Ruessink, B.G., 2012. Turbulence dissipation under breaking waves and bores in a natural surf zone. Cont. Shelf Res. 43, 133–141. https://doi.org/10.1016/j.csr.2012.05.014.

Guo, X., Shen, L., 2013. Numerical study of the effect of surface waves on turbulence underneath. Part 1. Mean flow and turbulence vorticity. J. Fluid Mech. 733, 558–587. https://doi.org/10.1017/jfm.2013.451.
Hatori, M., Tokuda, M., Toba, Y., 1981. Experimental study on strong interaction between regular waves and wind waves—I. J. Oceanogr. Soc. Jpn. 37, 111–119. https://doi.org/10.1007/BF02308095.
Henriquez, M., Reniers, A.J.H.M., Ruessink, B.G., Stive, M.J.F., 2014. PIV measurements of the bottom boundary layer under nonlinear surface waves. Coast. Eng. 94, 33–46. https://doi.org/10.1016/j.coastaleng.2014.08.004.
Hooshmand, A., Horner-Devine, A.R., Lamb, M.P., 2015. Structure of turbulence and sediment stratification in wave-supported mud layers. J. Geophys. Res. Oceans 120, 2430–2448. https://doi.org/10.1002/2014JC010231.
Imai, Y., Hatori, M., Tokuda, M., Toba, Y., 1981. Experimental Study on Strong Interaction between Regular Waves and Wind Waves—II 17.
Jiang, C., Yang, Y., Deng, B., 2020. Study on the nearshore Evolution of regular waves under steady wind. Water 12, 686. https://doi.org/10.3390/w12030686.
Jiang, J., Street, R.L., Klotz, S.P., 1990. A study of wave-turbulence interaction by use of a nonlinear water wave decomposition technique. J. Geophys. Res. 95, 16037–16054. https://doi.org/10.1029/JC095iC09p16037.
Kemp, P.H., Simons, R.R., 1983. The interaction of waves and a turbulent current: waves propagating against the current. J. Fluid Mech. 130, 73. https://doi.org/10.1017/S0022112083000981.
Kemp, P.H., Simons, R.R., 1982. The interaction between waves and a turbulent current: waves propagating with the current. J. Fluid Mech. 116, 227–250. https://doi.org/10.1017/S0022112082000445.
Lai, R.J., Shemdin, O.H., 1971. Laboratory investigation of air turbulence above simple water waves. J. Geophys. Res. 76, 7334–7350. https://doi.org/10.1029/JC076i030p07334.
Lamb, M.P., 2004. Turbulent structure of high-density suspensions formed under waves. J. Geophys. Res. 109, C12026. https://doi.org/10.1029/2004JC002355.
Lin, T., Gad-el-Hak, M., 1984. Turbulent current measurements in a wind-wave tank. J. Geophys. Res. 89, 627–636. https://doi.org/10.1029/JC089iC01p00627.
Liu, K., Chen, Q., Kaihatu, J.M., 2016. Modeling wind effects on shallow water waves. J. Waterw. Port, Coast. Ocean Eng. 142, 04015012. https://doi.org/10.1061/(ASCE)WW.1943-5460.0000314.
Longo, S., 2012. Wind-generated water waves in a wind tunnel: free surface statistics, wind friction and mean air flow properties. Coast. Eng. 61, 27–41. https://doi.org/10.1016/j.coastaleng.2011.11.008.
Longo, S., Liang, D., Chiapponi, L., Aguilera Jiménez, L., 2012. Turbulent flow structure in experimental laboratory wind-generated gravity waves. Coast. Eng. 64, 1–15. https://doi.org/10.1016/j.coastaleng.2012.02.006.
Longuet-Higgins, M.S., 1953. Mass transport in water waves. Phil. Trans. Roy. Soc. Lond. 245, 535–581. https://doi.org/10.1098/rsta.1953.0006.
Mansard, E.P.D., Funke, E.R., 1980. The Measurement of Incident and Reflected Spectra Using a Least Squares Method, the 17th International Conference on Coastal Engineering. ASCE, Sydney, Australia, pp. 154–172. https://doi.org/10.1061/9780872622647.008.
Meirelles, S., Henriquez, M., Horner-Devine, A.R., Souza, A.J., Pietrzak, J., Stive, M., 2015. Bed shear stress on the middle shoreface of the south-Holland coast. In: The Proceedings of the Coastal Sediments 2015. Presented at the Coastal Sediments 2015. World Scientific, San Diego, USA. https://doi.org/10.1142/9789814689977_0210.
Mellor, G., 2013. Pressure–slope momentum transfer in ocean surface boundary layers coupled with gravity waves. https://doi.org/10.1175/JPO-D-13-068.1.
Moghimi, S., Thomson, J., Özkan-Haller, T., Umlauf, L., Zippel, S., 2016. On the modeling of wave-enhanced turbulence nearshore. Ocean Modelling, Waves and coastal, regional and global processes 103, 118–132. https://doi.org/10.1016/j.ocemod.2015.11.004.
Nielsen, P., Teakle, I.A.L., 2004. Turbulent diffusion of momentum and suspended particles: a finite-mixing-length theory. Phys. Fluids 16, 2342–2348. https://doi.org/10.1063/1.1738413.
Nielsen, P., 1992. Coastal Bottom Boundary Layers and Sediment Transport. World Scientific.
Nishino, S., Kawaguchi, Y., Inoue, J., Yamamoto-Kawai, M., Aoyama, M., Harada, N., Kikuchi, T., 2020. Do strong winds impact water mass, nutrient, and phytoplankton distributions in the ice-free Canada basin in the fall? J. Geophys. Res. Oceans 125. https://doi.org/10.1029/2019JC015428.
Olfateh, M., Ware, P., Callaghan, D.P., Nielsen, P., Baldock, T.E., 2017. Momentum transfer under laboratory wind waves. Coast. Eng. 121, 255–264. https://doi.org/10.1016/j.coastaleng.2016.09.001.
Peruzzi, C., Vettori, D., Poggi, D., Blondeaux, P., Ridolfi, L., Manes, C., 2021. On the influence of collinear surface waves on turbulence in smooth-bed open-channel flows. J. Fluid Mech. 924, A6. https://doi.org/10.1017/jfm.2021.605.
Qiao, F., Yuan, Y., Yang, Y., Zheng, Q., Xia, C., Ma, J., 2004. Wave-induced mixing in the upper ocean: distribution and application to a global ocean circulation model. Geophys. Res. Lett. 31. https://doi.org/10.1029/2004GL019824.
Qiao, F., Fang, G., Xia, C., Yang, Y., Ma, J., Yuan, Y., 2008. The role of surface waves in the ocean mixed layer. Acta Oceanol. Sin. 3, 30–37.
Qiao, F., Yuan, Y., Deng, J., Dai, D., Song, Z., 2016. Wave–turbulence interaction-induced vertical mixing and its effects in ocean and climate models. Phil. Trans. R. Soc. A 374, 20150201. https://doi.org/10.1098/rsta.2015.0201.
Rainville, L., Lee, C., Woodgate, R., 2011. Impact of wind-driven mixing in the arctic ocean. Oceanog 24, 136–145. https://doi.org/10.5670/oceanog.2011.65.
Rainville, L., Woodgate, R.A., 2009. Observations of internal wave generation in the seasonally ice-free Arctic. Geophys. Res. Lett. 36, L23604. https://doi.org/10.1029/2009GL041291.
Reynolds, W.C., Hussain, A.K.M.F., 1972. The mechanics of an organized wave in turbulent shear flow. Part 3. Theoretical models and comparisons with experiments. J. Fluid Mech. 54, 263–288. https://doi.org/10.1017/S0022112072000679.
Savelyev, I.B., Haus, B.K., Donelan, M.A., 2011. Experimental study on wind-wave momentum flux in strongly forced conditions. J. Phys. Oceanogr. 41 (1), 1328–1344. https://doi.org/10.1175/2011JPO4577.
Savelyev, I.B., Maxeiner, E., Chalikov, D., 2012. Turbulence production by nonbreaking waves: laboratory and numerical simulations: wave-induced turbulence. J. Geophys. Res. 117. https://doi.org/10.1029/2012JC007928 n/a-n/a.
Smeltzer, B.K., Rømcke, O., Hearst, R.J., Ellingsen, S.Å., 2023. Experimental study of the mutual interactions between waves and tailored turbulence. J. Fluid Mech. 962, R1. https://doi.org/10.1017/jfm.2023.280.
Soulsby, R.L., Humphery, J.D., 1990. Field observations of wave-current interaction at the sea bed. In: Tørum, A., Gudmestad, O.T. (Eds.), Water Wave Kinematics. Springer, Netherlands, Dordrecht, pp. 413–428. https://doi.org/10.1007/978-94-009-0531-3_25.
Sous, D., Forsberg, P.L., Touboul, J., Gonçalves Nogueira, G., 2021. Laboratory experiments of surf zone dynamics under on- and offshore wind conditions. Coast. Eng. 163, 103797. https://doi.org/10.1016/j.coastaleng.2020.103797.
Sous, D., Forsberg, P.L., Touboul, J., Nogueira, G.G., 2020. Laboratory experiments of surf zone dynamics under on- and offshore wind conditions. Coast. Eng., 103797 https://doi.org/10.1016/j.coastaleng.2020.103797.
Su, M., Yao, P., Wang, Z.B., Chen, Y.P., Zhang, C.K., Stive, M.J.F., 2015. Laboratory Studies on the Response of Fine Sediment to Wind, p. 10.
Talke, S.A., Stacey, M.T., 2003. The influence of oceanic swell on flows over an estuarine intertidal mudflat in San Francisco Bay. Estuar. Coast Shelf Sci. 58, 541–554. https://doi.org/10.1016/S0272-7714(03)00132-X.
Teixeira, M.A.C., Belcher, S.E., 2002. On the distortion of turbulence by a progressive surface wave. J. Fluid Mech. 458, 229–267. https://doi.org/10.1017/S0022112002007838.
Thais, L., Magnaudet, J., 1995. A triple decomposition of the fluctuating motion below laboratory wind water waves. J. Geophys. Res. 100, 741. https://doi.org/10.1029/94JC02714.
Thais, L., Magnaudet, J., 1996. Turbulent structure beneath surface gravity waves sheared by the wind. J. Fluid Mech. 328, 313–344. https://doi.org/10.1017/S0022112096008749.
Ting, F.C.K., Kirby, J.T., 1994. Observation of undertow and turbulence in a laboratory surf zone. Coast. Eng. 24, 51–80. https://doi.org/10.1016/0378-3839(94)90026-4.
Wei, L., Guan, C., Troitskaya, Y., 2018. Laboratory experiment on wave induced turbulence. J. Ocean Univ. China 17, 721–726. https://doi.org/10.1007/s11802-018-3528-4.
Xuan, A., Shen, L., 2023. Reconstruction of three-dimensional turbulent flow structures using surface measurements for free-surface flows based on a convolutional neural network. J. Fluid Mech. 959, A34. https://doi.org/10.1017/jfm.2023.154.
Yao, P., Su, M., Wang, Z.B., van Rijn, L.C., Zhang, C.K., Chen, Y.P., Stive, M.J.F., 2015. Experiment inspired numerical modeling of sediment concentration over sand–silt mixtures. Coast. Eng. 105, 75–89. https://doi.org/10.1016/j.coastaleng.2015.07.008.
Zdyrski, T., Feddersen, F., 2022. Wind-induced changes to shoaling surface gravity wave shape. Phys. Rev. Fluids 7, 074802. https://doi.org/10.1103/PhysRevFluids.7.074802.
Zhang, M., Dai, Z., Bouma, T.J., Bricker, J., Townend, I., Wen, J., Zhao, T., Cai, H., 2021. Tidal-flat reclamation aggravates potential risk from storm impacts. Coast. Eng. 166, 103868. https://doi.org/10.1016/j.coastaleng.2021.103868.